# CD24 is expressed by myofiber synaptic nuclei and regulates synaptic transmission

**Marko Jevsek*, Alexander Jaworski*, Luis Polo-Parada†, Natalie Kim*, Jihua Fan*, Lynn T. Landmesser†‡, and Steven J. Burden*‡**

*Molecular Neurobiology Program, Skirball Institute of Biomolecular Medicine, New York University Medical School, New York, NY 10016; and †Department of Neurosciences, School of Medicine, Case Western Reserve University, Cleveland, OH 44106

Contributed by Lynn T. Landmesser, February 22, 2006

**The genes encoding several synaptic proteins, including acetylcholine receptors, acetylcholinesterase, and the muscle-specific kinase, MuSK, are expressed selectively by a small number of myofiber nuclei positioned near the synaptic site. Genetic analysis of mutant mice suggests that additional genes, expressed selectively by synaptic nuclei, might encode muscle-derived retrograde signals that regulate the differentiation of motor axon terminals. To identify candidate retrograde signals, we used a microarray screen to identify genes that are preferentially expressed in the synaptic region of muscle, and we analyzed one such gene, *CD24*, further. We show that *CD24*, which encodes a small, variably and highly glycosylated, glycosylphosphatidylinositol (GPI)-linked protein, is expressed preferentially by myofiber synaptic nuclei in embryonic and adult muscle, and that *CD24* expression is restricted to the central region of muscle independent of innervation. Moreover, we show that CD24 has a role in presynaptic differentiation, because synaptic transmission is depressed and fails entirely, in a cyclical manner, after repetitive stimulation of motor axons in *CD24* mutant mice. These deficits in synaptic transmission, which are accompanied by aberrant stimulus-dependent uptake of AM1–43 from axons, indicate that CD24 is required for normal presynaptic maturation and function. Because *CD24* is also expressed in some neurons, additional experiments will be required to determine whether pre- or postsynaptic CD24 mediates these effects on presynaptic development and function.**

heat-stable antigen | neuromuscular synapses | P-selectin | synapse-specific transcription

Nearly one dozen genes, including those encoding acetylcholine receptors (AChRs), acetylcholinesterase (AChE), muscle-specific kinase (MuSK), and utrophin, are expressed selectively by a small number of myofiber nuclei positioned near the synaptic site (1–5). This pattern of gene expression depends on MuSK, a muscle-specific receptor tyrosine kinase that is activated by neurally derived agrin, because "synapse-specific" genes are expressed uniformly in muscle from *MuSK* mutant mice (6). In addition, presynaptic differentiation is MuSK-dependent, because motor axons fail to stop and differentiate in *agrin* or *MuSK* mutant mice (6, 7). Because MuSK is required for synapse-specific transcription and presynaptic differentiation, these findings raise the possibility that muscle-derived signals, which cause motor axons to stop growing and differentiate, may be expressed preferentially by myofiber synaptic nuclei.

Among the known synapse-specific genes, *AChR*, *AChE*, *MuSK*, *NCAM*, and *S-laminin* encode for cell surface proteins, suggesting that these proteins could, in principle, function as retrograde signals (1–3, 5, 8). It seems likely, however, that additional genes, encoding cell surface proteins, are transcribed preferentially by myofiber synaptic nuclei. In mammalian muscle, neuromuscular synapses are confined to a narrow zone, near the center of the muscle. As such, the synaptic region of the muscle can be dissected from the nonsynaptic region (9). Although the dissected synaptic region contains far more nonsynaptic than synaptic nuclei (1), a comparison of RNA expressed in the two regions can identify RNAs that are enriched in the myofiber synaptic region. To identify candidate retrograde signals, we screened oligonucleotide microarrays with synaptic and nonsynaptic RNA, and we found that *CD24* (10, 11), which encodes a small, mucin-type glycosylphosphatidylinositol-linked protein, is enriched in the synaptic region of muscle. We studied the pattern of *CD24* expression in muscle from wild-type mice and mutant mice lacking Schwann cells, and we show that *CD24* is expressed by myofiber synaptic nuclei in embryonic and adult muscle. Further, we show that *CD24* expression is restricted to the central region of muscle independent of innervation. We analyzed *CD24* mutant mice and demonstrate that CD24 is required for appropriate presynaptic function, because repetitive stimulation of motor axons leads to synaptic depression and total transmission failures in mutant, but not control, mice. These physiological deficits are accompanied by alterations in the uptake of AM1–43, indicating that CD24 is also required for the normal cycling of synaptic vesicles.

## Results

**A Microarray Screen for Synaptic RNAs Identifies *CD24*.** In mammalian muscle, motor axons terminate and form synapses with myofibers in the central region of the muscle. We dissected diaphragm muscles from postnatal day 16 (P16) mice into synaptic and nonsynaptic regions, isolated RNA from each region, and probed Affymetrix microarrays with synaptic and nonsynaptic cDNA (see *Materials and Methods*).

We considered further those RNAs that were ≥3-fold more abundant in the synaptic than nonsynaptic region. As synaptic nuclei constitute ≈1% of the ≈500 nuclei within individual myofibers, the dissected synaptic region still contains far more (≈25-fold) nonsynaptic than synaptic nuclei. Therefore, assuming a similar rate of mRNA degradation in synaptic and nonsynaptic regions, a 3-fold enrichment corresponds to a 50-fold increase in the rate of transcription from individual synaptic nuclei. The signals for RNAs that are expressed less selectively by synaptic nuclei (e.g., *rapsyn*, *utrophin*, *S-laminin*, and *MuSK*) (8) were not appreciably and reliably different in microarrays probed with synaptic and nonsynaptic cDNA.

Because we sought to identify candidate retrograde signals for presynaptic differentiation, we chose to analyze genes that encode for secreted or membrane-bound proteins. *CD24* was the only gene, which we identified, that met this criterion and was

Conflict of interest statement: No conflicts declared.

Freely available online through the PNAS open access option.

Abbreviations: α-BGT, α-bungarotoxin; AChRs, acetylcholine receptors; E*n*, embryonic day *n*; EPP, endplate potential; MBP, myelin basic protein; MEPP, miniature endplate potential; MLC, myosin light chain; MLCK, MLC kinase; MuSK, muscle-specific kinase; NCAM, neural cell adhesion molecule; Nrg-1, Neuregulin-1; P*n*, postnatal day *n*.

Data deposition: The sequence reported in this paper has been deposited in the GenBank database (accession no. NM_009846).

‡To whom correspondence may be addressed. E-mail: lynn.landmesser@case.edu or burden@saturn.med.nyu.edu.

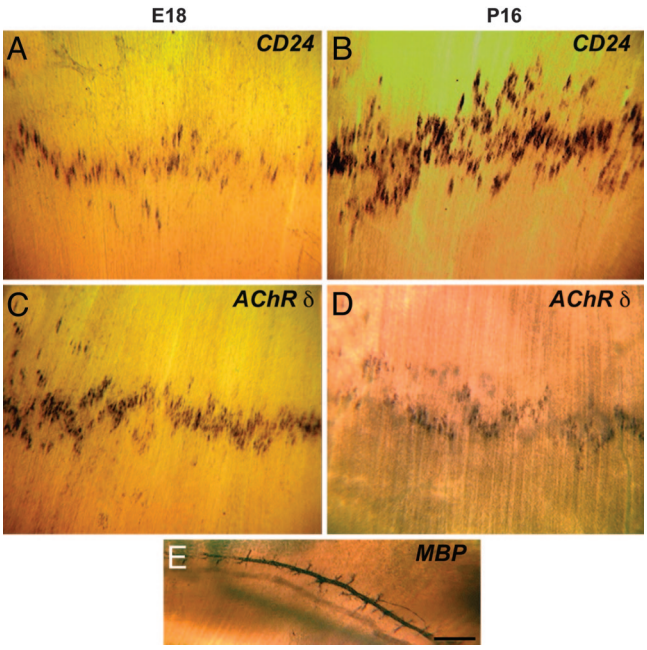


**Fig. 1.** *CD24* mRNA is concentrated in the central region of muscle. Whole mounts of diaphragm muscles from wild-type E18 embryos (*A* and *C*) and P16 mice (*B*, *D*, and *E*) were processed for *in situ* hybridization by using a probe for *CD24* (*A* and *B*), *AChR* δ subunit (*C* and *D*), or *myelin basic protein* (*MBP*) (*E*), respectively. *CD24* RNA, like *AChR* RNA, is concentrated in the central, synaptic region of embryonic and postnatal muscle. Although the level of *AChR* δ subunit expression decreases after birth, *CD24* expression appears to increase postnatally. *MBP* is expressed in myelinating Schwann cells, associated with axons. Although *MBP* expression is enriched in the central region of the muscle, the pattern of *MBP* expression is distinctly different from the patterns of *CD24* or *AChR* expression. (Scale bar: 200 μm.)

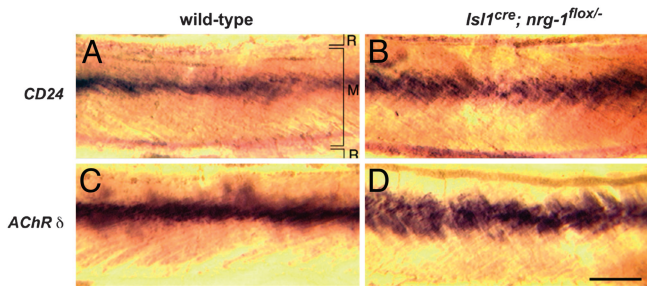


**Fig. 2.** *CD24* mRNA is concentrated in the myofiber synaptic region. Whole mounts of intercostal muscles from wild-type (*A* and *C*) and $Isl1^{cre}$;$nrg\text{-}1^{flox/-}$ (*B* and *D*) E18 embryos were processed for *in situ* hybridization by using probes for *CD24* (*A* and *B*) and *AChR* δ subunit (*C* and *D*), respectively. *CD24*, like *AChR* δ, is expressed preferentially in the central region of muscle from neuronal *nrg-1* mutant embryos (*B* and *D*). As neuronal *nrg-1* mutant embryos lack Schwann cells, these results indicate that *CD24* is expressed by myofiber synaptic nuclei. The positions of the ribs (R) and muscle (M) are indicated in *A*. (Scale bar: 200 μm.)

reproducibly more abundant (≥3-fold) in the synaptic region. In three separate microarray experiments, *CD24* was enriched 3.6 ± 0.40-fold (mean ± SEM, $n = 3$) in the synaptic region, similar to that for *acetylcholine receptor* (*AChR*) α subunit (3.5 ± 0.34-fold) and *acetylcholinesterase* (3.8 ± 0.62-fold) genes, but less than the *AChR epsilon* subunit gene (8.8 ± 2.92-fold).

***CD24* Is Expressed Preferentially by Myofiber Synaptic Nuclei.** To determine whether *CD24* RNA is indeed enriched in the synaptic region of muscle, we studied *CD24* expression by *in situ* hybridization. Fig. 1 shows that *CD24* RNA, like *AChR* RNA, is concentrated in the central region of muscle from P16 and embryonic day 18.5 (E18.5) mice, validating the results from the microarray screen.

We considered three possible cellular sources for *CD24* expression in muscle: myelinating Schwann cells, terminal Schwann cells, or synaptic nuclei of myofibers. Myelinating Schwann cells, which are associated with axons, are indeed enriched in the central region of muscle, as indicated by the elevated expression of *myelin basic protein* (*MBP*) (8.4 ± 1.58-fold) and *myelin protein P0* (12.4 ± 3.50-fold) in the dissected synaptic region and by the expression pattern of *MBP* in muscle (Fig. 1). Nonetheless, the pattern of *MBP* expression is distinctly different from *CD24* or *AChR* genes, indicating that myelinating Schwann cells cannot account for the pattern of *CD24* expression in muscle.

Terminal Schwann cells are associated with nerve terminals but not motor axons. We cannot distinguish expression from terminal Schwann cells and myofiber synaptic nuclei by *in situ* hybridization of muscle whole mounts (12). Thus, our *in situ* hybridization data are consistent with the possibility that *CD24* is expressed in terminal Schwann cells or in myofiber synaptic nuclei. To distinguish between these possibilities, we examined the pattern of *CD24* expression in muscle from a mutant mouse line lacking intramuscular Schwann cells. Neuregulin-1 (Nrg-1) is a neuronally derived ligand required for Schwann cell survival; in its absence, Schwann cells die and are therefore absent from intramuscular axons (13). We analyzed *CD24* expression in muscle from $Isl1^{cre/+}$;$nrg^{f/-}$ embryos, which lack neuronal Nrg-1, and from control littermates (13). Fig. 2 shows that the pattern of *CD24* expression is identical in wild-type and mutant embryos lacking terminal Schwann cells. Taken together, these data indicate that *CD24* is expressed preferentially by myofiber synaptic nuclei. Moreover, these findings demonstrate that *CD24* is expressed by myofiber synaptic nuclei in embryonic (E18.5), as well as in postnatal, muscle.

***CD24* Expression Is Patterned in Muscle Independent of Innervation.** In the absence of innervation, *AChR* genes are expressed preferentially in the central region of muscle (13–15). These findings suggest that muscle prepatterning may establish a preferred region for motor innervation. To determine whether *CD24* expression is patterned independent of innervation, we examined *CD24* expression in muscle from embryos lacking motor neurons. Mice that carry $Isl2^{loxP\text{-}stop\text{-}loxP\text{-}DTA}$ and $HB9^{cre}$ alleles express diphtheria toxin selectively in motor neurons, causing these motor neurons to die as soon as they exit the cell cycle and before they extend axons into the muscle (13). We studied *CD24* expression in $Isl2^{loxP\text{-}stop\text{-}loxP\text{-}DTA}$;$HB9^{cre}$ embryos and found that *CD24* expression, like *AChR* expression, is enriched in the central region of muscle lacking motor axons (Fig. 3). Thus, *CD24* expression is patterned in muscle independent of motor innervation. Neural signals, however, refine this pattern of *CD24* expression, because the width of the *CD24* expressing zone, like the *AChR* zone, is wider in muscle lacking motor axons than in innervated muscle (Fig. 3). Moreover, these data provide additional evidence that myofiber synaptic nuclei are responsible for the enrichment of *CD24* RNA in innervated muscle, because $Isl2^{loxP\text{-}stop\text{-}loxP\text{-}DTA}$;$HB9^{cre}$ embryos, like $Isl1^{cre/+}$;$nrg^{f/-}$ mice, lack intramuscular Schwann cells (13).

**Neuromuscular Synapses Exhibit Normal Morphology in *CD24* Mutant Mice.** *CD24* mutant mice are viable and fertile, indicating that CD24 is not essential for neuromuscular function (16). To determine whether *CD24* mutant synapses appear normal, we stained whole mounts of muscle from *CD24* mutant mice with antibodies to neurofilament and synaptophysin to visualize axons and nerve terminals, respectively, and with Alexa 594 α-bunga-

NEUROSCIENCE

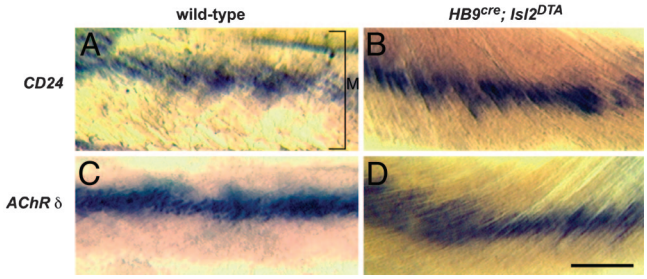


**Fig. 3.** *CD24* expression is patterned in the absence of innervation. Whole mounts of intercostal muscles from E18.5 wild-type (*A* and *C*) and *HB9*$^{cre}$;*Isl2*$^{DTA}$ (*B* and *D*) embryos were processed for *in situ* hybridization by using probes for *CD24* (*A* and *B*) and *AChR* δ subunit (*C* and *D*), respectively. *CD24* expression, as well as *AChR* δ expression, is patterned in the central region of muscle from wild-type and *HB9*$^{cre}$;*Isl2*$^{DTA}$ mice, indicating that *CD24* expression is patterned independent from innervation. The width of the *CD24*-expressing zone, like the AChR expressing zone, is narrower in wild-type embryos (*A* and *C*) than in embryos lacking motor neurons (*B* and *D*). (Scale bar: 200 μm.)

rotoxin (α-BGT) to mark AChRs. We found that axon growth and branching, as well as the shape of nerve terminals in diaphragm muscle, appear normal in *CD24* mutant mice and control littermates (Fig. 4). Moreover, the size of synapses and the density of synaptic AChRs are similar in *CD24* mutant and control mice (Table 1; Fig. 7, which is published as supporting information on the PNAS web site). In addition, muscle fibers were singly innervated, indicating that the process of neonatal synapse elimination had proceeded normally (Movies 1 and 2, which are published as supporting information on the PNAS web site). Thus, at least by these criteria, neuromuscular synapses appear normal in *CD24* mutant mice.

**Synaptic Transmission Is Defective in *CD24* Mutant Mice.** In wild-type adult mice, stimulation of the muscle nerve leads to reliable and efficient release of neurotransmitter, and the response or endplate potential (EPP) is maintained even at high stimulation (100 Hz) frequencies (Fig. 5*A*). In *CD24* mutant mice, effective transmission was maintained at low stimulation frequencies (10 Hz) (Fig. 5*A*). Miniature endplate potential (MEPP) frequency did not differ significantly from wild-type, nor did MEPP amplitude (Fig. 5*B*), the latter confirming the normal density of postsynaptic AChRs reported in Table 1. These observations indicate that the basic machinery for synaptic transmission

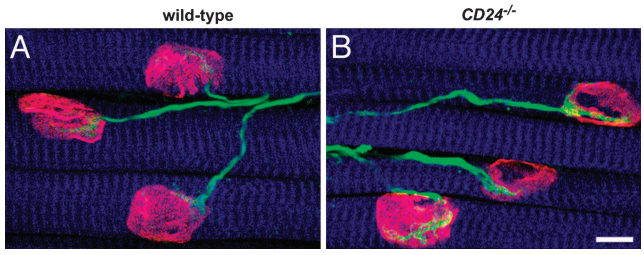


**Fig. 4.** Neuromuscular synapses in *CD24* mutant mice appear morphologically normal. Whole mounts of diaphragm muscles from wild-type (*A*) and *CD24* mutant (*B*) P11 mice were stained with antibodies to neurofilament and synaptophysin to visualize motor axons and nerve terminals (green), Alexa 594–α-BGT to label postsynaptic AChRs (red), and Alexa 660–phalloidin to visualize muscle fibers (blue). In wild-type and *CD24* mutant mice, the main intramuscular nerve is positioned in the middle of the muscle and oriented perpendicular to the muscle fibers. AChR clusters are concentrated at synaptic sites both in wild-type and *CD24* mutant mice (*A* and *B*). The shape and size of synaptic AChR clusters are similar in wild-type and *CD24* mutant mice (*A* and *B*). (Scale bar: 200 μm.)

**Table 1. The size of synaptic AChR clusters, the density of synaptic AChRs, as well as the elimination of synapses are normal in *CD24* mutant mice**

| | *CD24*$^{-/-}$ | Wild type |
|---|---|---|
| Size of synaptic AChR clusters | 442 ± 23 μm$^3$ | 406 ± 19 μm$^3$ |
| | 543 ± 27 μm$^3$ | 464 ± 23 μm$^3$ |
| AChR density | 492 ± 14 | 489 ± 16 |
| | 524 ± 17 | 487 ± 13 |
| Multiply innervated synapses | 5.6% (6/108) | 6.3% (6/95) |
| | 6.7% (10/149) | 6.0% (7/116) |

Whole mounts of diaphragm muscles from wild-type and *CD24* mutant mice, at P11, were stained with antibodies to neurofilament and synaptophysin and Alexa 594–α-BGT. Three-dimensional reconstructions of image stacks were analyzed to measure the size of synaptic AChR clusters (number of voxels) and the average density of AChRs within these clusters (total grayscale value/number of voxels). We measured synaptic size and AChR density at ≥25 synapses in two mice from each genotype; the mean ± SEM in each mouse is indicated. The extent of polyneural innervation was measured by rotating three-dimensional reconstructions and counting the number of axons that project into individual synaptic sites (Movies 1 and 2). We calculated the extent of polyneuronal innervation at ≥95 synapses in two mice from each genotype; the percentage of synaptic sites that were multiply innervated in each mouse is indicated.

remains intact in *CD24* mutant mice. However, as the stimulation frequency was increased, total transmission failures became apparent at 20 Hz and increased in number with increasing stimulation rates (Fig. 5 *A* and *B*). At 100-Hz stimulation, the *CD24* mutant junctions exhibited periodic bouts of total transmission failures that were interspersed with periods of transmission but with depressed EPP amplitude. In addition, quantal content to single stimuli was significantly reduced (Fig. 5*B*). Despite these alterations in transmission, the size of *CD24* mutant semitendinosus endplates is normal (Fig. 7). These observations indicate presynaptic deficits in transmission in *CD24* mutant junctions, specifically in their ability to maintain effective transmission with repetitive stimulation at moderate to high frequencies that are typical for the firing rate of fast motor neurons.

**The Transmission Defects in CD24 Mutant Junctions Are Similar to Neural Cell Adhesion Molecule (NCAM) Mutant Junctions and May Be Caused by a Similar Mechanism.** These unusual cyclical bouts of total transmission failure at high frequency of stimulation bear striking similarity to junctions lacking the 180 isoform of NCAM (17). However, unlike *NCAM 180* isoform mutant mice, but similar to mice that lack all NCAM isoforms (18), EPP amplitudes were also depressed at higher stimulation rates (Fig. 5*A*). Previous studies have shown that these transmission failures are not produced by failure of the endplate to be depolarized because of branch point failures of action potential propagation (18, 19). Because mouse neuromuscular junctions are not invaded by the action potential but are electrotonically depolarized by currents from the last node of Ranvier (20), such currents, including $Ca^{2+}$ currents from the presynaptic terminal, can be measured with extracellular recordings, and these currents were not altered with frequencies of repetitive stimulation that produced transmission failures. These transmission failures thus appear to result from some defect downstream of $Ca^{2+}$ entry, and evidence suggests that the *NCAM* mutant junctions are unable to effectively mobilize synaptic vesicles from the reserve pool to presynaptic release sites. This idea is supported by capacitance/amperometry measurements of chromaffin granule exocytosis with repetitive stimulation in *NCAM* mutant mice (21).

By introducing specific blocking and activating peptides into wild-type nerve terminals in isolated semitendinosus muscles, Polo-Parada and colleagues (19) recently demonstrated that the defects in transmission in the 180 isoform-deficient mice ap-

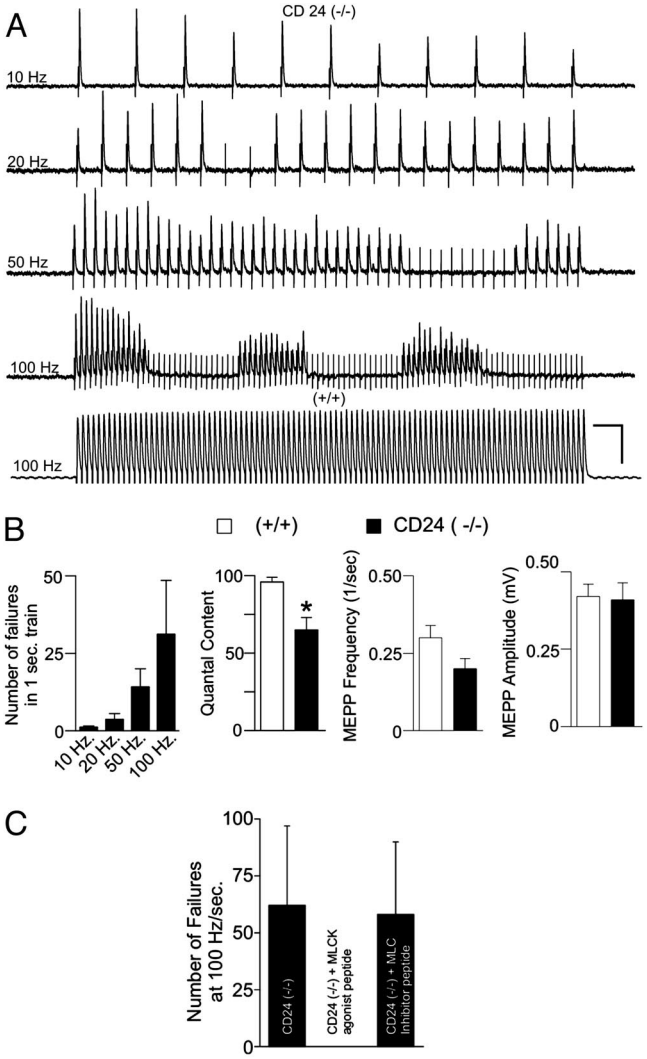


**Fig. 5.** Defects in synaptic transmission in *CD24* mutant mice. (*A*) EPPs, which were recorded from *CD24* mutant junctions in response to stimulus trains at different stimulus frequencies, reveal periods of total transmission failures at ≥20 Hz, as well as depression in EPP amplitude at the higher frequencies (calibration = 50 msec and 15 mV). No failures were detected in wild-type littermates at any frequency, as the 100-Hz example (*A*) illustrates. (*B*) Quantification of transmission parameters at *CD24* mutant (black bars) and wild-type (white bars) junctions showing the number of failures within a 1-sec train at different stimulation frequencies ($n$ = 28 cells), and the quantal content (calculated for four cells as the mean EPP amplitude/mean MEPP amplitude), MEPP frequency, and MEPP amplitude (each calculated from 12 cells with at least 500 MEPPs from each cell). Quantal content at *CD24* mutant junctions was significantly depressed compared with wild-type ($P < 0.005$). Data are expressed as mean ± SEM. (*C*) The number of transmission failures during a 1 sec, 100 Hz stimulus train in *CD24* mutant endplates and in *CD24* mutant junctions after the introduction of an MLCK agonist peptide and a peptide that inhibits MLC ($n$ = 28 cells). The MLCK agonist peptide completely rescued the transmission failures, whereas the MLC inhibitory peptide did not produce additional failures.

peared to result from inadequate activation of myosin light chain kinase (MLCK) and in turn myosin light chain (MLC) and myosin II, because interfering with this pathway in wild-type mice mimicked the transmission defects. Activation of this pathway appears necessary to replenish synaptic vesicles used during high frequency stimulation (19). Thus, in *NCAM* mutant junctions, the failure of MLCK to be sufficiently activated appears to produce the observed transmission failures, because

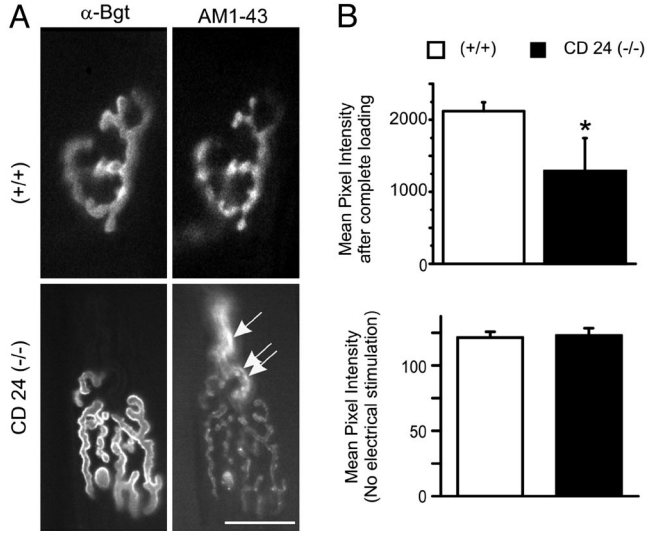


**Fig. 6.** Alterations in AM1–43 uptake in *CD24* mutant junctions. (*A*) Examples of wild-type and *CD24* mutant terminals stained with rhodamine-conjugated α-BGT to visualize the endplate and AM1–43 to visualize synaptic vesicles that have been loaded after a 10-min stimulation of the muscle nerve at 10 Hz, a protocol previously shown to result in optimal labeling of the pool of cycling vesicles. Arrows indicate sites of aberrant uptake along the preterminal axon in the *CD24* mutant terminals, whereas uptake at the wild-type junction is precisely confined to the junction as defined by α-BGT staining. (Scale bar: 40 μm.) (*B*) Quantification of AM1–43 uptake in *CD24* mutant ($n$ = 17; black bars) and wild-type ($n$ = 17; white bars) junctions. Mean pixel intensity after a 10 sec, 10 Hz loading protocol is significantly reduced in *CD24* mutant junctions ($P < 0.005$) (*Upper*). Loading for 10 min in the absence of electrical stimuli was minimal and did not differ between *CD24* mutant and wild-type junctions. Data are expressed as mean ± SEM.

these failures can be rescued by making MLCK constitutively active.

We therefore used similar methods to determine whether the transmission failures in *CD24* mutant junctions resulted from defects in this same signaling pathway. Acute introduction of a peptide that activates MLCK and rescues the transmission failures in *NCAM* mutant mice (19) also completely prevented the transmission failures at *CD24* mutant junctions (Fig. 5*C*). In addition, a peptide inhibitor of MLC that produces transmission failures at wild-type junctions (19) did not produce additional failures in *CD24* mutant mice (Fig. 5*C*). Taken together, these data indicate defects in the MLCK signaling pathway that are likely to underlie the transmission failures in *CD24* mutant mice.

In mice lacking all NCAM isoforms, synaptic vesicle exocytosis and synaptic vesicle endocytosis are not confined to the endplate proper but occur along the length of the preterminal axon. Using AM1–43 (analogous to FM1–43) to fully load the cycling pool of vesicles, we found that, whereas in wild-type junctions dye uptake was precisely confined to the endplate (Fig. 6*A Upper Right*), stimulus-dependent uptake along the preterminal axon was evident in *CD24* mutant junctions (Fig. 6*A Lower Right*). There was minimal uptake of AM1–43 in the absence of stimulation, and this uptake did not differ between wild-type and *CD24* mutant junctions (Fig. 6*B Lower*). However, stimulus-dependent loading of dye for 10 min (sufficient to label the entire cycling pool) revealed that the size of this vesicle pool was significantly decreased in *CD24* mutant mice (Fig. 6*B Upper*). Moreover, in *CD24* mutant mice, the pattern of AM1–43 uptake was unusual. In wild-type terminals (Fig. 6*A*), sites of dye uptake are widespread, resulting in intense, distributed labeling within much of the terminal (17, 18). In *CD24* mutant terminals, bright puncta of dye were more sparsely distributed (Fig. 6*A*). These

NEUROSCIENCE

observations indicate that the size of the cycling vesicle pool is smaller in *CD24* mutant terminals and suggest that there may be fewer active zones. These alterations could contribute to the reduction in quantal content and to the observed transmission failures.

## Discussion

Our experiments demonstrate that *CD24* RNA accumulates in the synaptic region of skeletal myofibers. Consistent with our findings, a similar microarray screen also found *CD24* to be enriched in the central region of adult muscle (22). *CD24* is the first RNA encoding a glycosylphosphatidylinositol-linked protein, shown to be enriched in the synaptic region of muscle and, like *AChR* genes, is expressed selectively in the central region of muscle independent of innervation.

We demonstrated that CD24 has a role, direct or indirect, in synaptic transmission. In its absence, junctions exhibited both synaptic depression and cyclical periods of total transmission failures. In addition, the size of the pool of recycling vesicles in the terminal was reduced compared with wild-type junctions, and stimulus-dependent vesicle cycling was not confined to the endplate but also occurred along the preterminal axon, indicating a failure to properly target vesicle release machinery. Because CD24 binds to L1 (23), an interaction between CD24 and motor neuron L1 during initial contact might generate a signal required for aspects of subsequent synaptic maturation. Alternatively, or in addition, CD24 might be required at adult junctions to maintain effective transmission.

The transmission failures are strikingly similar to those found in *NCAM* mutant mice (18). We therefore explored whether the synaptic defects in *CD24* mutant mice might arise from a similar mechanism. Strongly supporting this idea was our finding that a peptide activator of MLCK (19) completely rescued the transmission failures in *CD24* as well as *NCAM* mutant mice. Moreover, a peptide that inhibits MLC phosphorylation did not produce additional failures in *CD24* mutant mice. Although other mechanisms may contribute to the phenotype, one possibility is that CD24 and NCAM are each required to activate a myosin-driven process that replenishes synaptic vesicles used during high frequency stimulation. This hypothesis is consistent with recent studies of exocytosis in the *Drosophila* neuromuscular junction (24) and in chromaffin cells lacking NCAM (21). That CD24 also affects processes mediated by NCAM isoforms in addition to the 180 isoform is suggested by the fact that depression of EPP amplitude with repetitive stimulation and the stimulus-dependent vesicle cycling along the preterminal axon, observed in *CD24* mutant mice, occur in junctions lacking all NCAM but not in those lacking only the 180 isoform.

How might the absence of CD24 or NCAM result in similar phenotypes? One possibility is that CD24 might regulate the expression or distribution of one or more NCAM isoforms. Although Western blots of wild-type and *CD24* mutant sciatic nerves did not reveal obvious differences in levels of NCAM isoform expression, and pan-NCAM immunostaining appeared similar at wild-type and *CD24* mutant neuromuscular junctions (L.P-P, unpublished observations), the distribution of NCAM isoforms within microdomains at the synapse might be altered. Given that CD24 has been reported to bind to a related cell adhesion molecule L1 (23), CD24 may also bind to one or more isoforms of NCAM. Alternatively, both CD24 and NCAM may act independently but cooperatively to engage a common signaling pathway such as MLCK. Clearly many additional experiments will be required to distinguish among these possibilities.

Finally, although our data are consistent with the idea that muscle-derived CD24 regulates synaptic transmission and vesicle cycling, we cannot exclude the possibility that motor neurons may express *CD24* and that CD24 may function autonomously in motor neurons to regulate synaptic transmission. CD24 is indeed expressed in developing neurons and implicated in regulating neuronal proliferation, neuronal migration, and neurite extension (25–27). Nonetheless, the *in vivo* role for CD24 in the nervous system is poorly understood (25). In contrast, the role for CD24 in leukocytes has been studied in more detail. CD24 is expressed in leukocytes and is required for rolling adhesion of leukocytes on endothelial cells and platelets (28). Rolling adhesion of leukocytes is mediated by P-selectin, which is expressed by endothelial cells and activated platelets and which binds the mucin domain of CD24 (28). It is not known whether this adhesive interaction is accompanied by intracellular signaling, but engagement of other glycosylphosphatidylinositol-linked proteins in T cells leads to recruitment and activation of Src family kinases, enhancing T cell receptor signaling (29), and antibody-mediated cross-linking of CD24 also activates Src family kinases (30). Thus, engagement of CD24 in presynaptic terminals, potentially through cis-interactions with NCAM (31), may stimulate Src family kinases and modulate vesicle trafficking by catalyzing phosphorylation of proteins important for exocytosis or endocytosis of synaptic vesicles (32–34).

## Materials and Methods

**Microarray Screen.** The synaptic region from the diaphragm muscles of 21 P16 male mice was isolated by dissecting the central one-quarter of the left hemidiaphragm muscle in oxygenated L15 medium at 37°C. The remaining nonsynaptic region of the muscle was further dissected to exclude the myotendinous region, because certain synaptic proteins are enriched at myotendinous junctions. Synaptic RNA from seven diaphragm muscles was pooled and copied into cDNA; likewise, nonsynaptic RNA from seven diaphragm muscles was pooled and copied into cDNA. Each of three Affymetrix mouse genome 430 2.0 microarrays was probed with a pool of synaptic cDNA, and each of three microarrays was probed with a pool of nonsynaptic cDNA. The chips were scanned with an Affymetrix GeneChip Scanner 3000, and the raw data (http://arrayconsortium.tgen.org/np2/viewProject.do?action=viewProject&projectId=191) were processed with Affymetrix GCOS. The signals were normalized and analyzed by DCHIP (35), and we calculated the ratio of expression in synaptic/nonsynaptic region.

**Histochemistry.** We stained whole mounts of diaphragm muscle with antibodies and measured the size and density of synaptic AChRs, largely as described in ref. 36, by using VOLOCITY 3D software (Improvision, Lexington, MA). We determined the number of synaptic sites that were multiply innervated by assembling projections from a stack of images collected with a 63× objective on a Zeiss 510 confocal microscope and rotating the projections so that we could trace individual axons branching into single synaptic sites. Whole mounts of muscle were probed with digoxigenin-labeled RNA probes as described in ref. 36. The *CD24* RNA probe is complementary to nucleotides 279–722 in *CD24* (accession no. NM_009846). $Isl1^{cre/+};nrg^{f/-}$ and in $Isl2^{loxP\text{-}stop\text{-}loxP\text{-}DTA};HB9^{cre}$ embryos were analyzed at E18.5.

We stained frozen sections of muscle with rat monoclonal antibodies to murine CD24 (M1/69 and J11d; BD PharMingen) but failed to detect staining at neuromuscular synapses. These results raise several possibilities. First, CD24 protein may be expressed at very low levels, precluding detection. Second, the epitope recognized by these antibodies may be buried by the mucin/carbohydrate modifications to CD24. Third, synaptic CD24 may be cleaved and released from the membrane by a phospholipase, because the epitope is lost after phosphatidylinositol-specific phospholipase C cleavage (37).

**Electrophysiology.** Semitendinosus muscles, with the nerve supply intact, were isolated from adult (3- to 5-month-old) mice and immediately placed into well-oxygenated Tyrode's solution. Al-

though the diaphragm was used to identify *CD24*, the semitendinosus muscle was chosen for functional analysis because this muscle was used in previous studies demonstrating defects in transmission in *NCAM* mutant mice (17, 18). In addition, we previously found that studying vesicle cycling via FM1–43 uptake was not possible in the diaphragm because of connective tissue that resulted in high background labeling. Standard intracellular recording procedures with sharp electrodes were carried out as described in refs. 17 and 18. The protocol for introducing peptides to interfere with specific presynaptic protein–protein interactions by using the peptide carrier Chariot (Active Motif, Carlsbad, CA) was described in ref. 19. Next, 500-$\mu$m longitudinal frozen sections stained with $\alpha$-BGT were used to characterize the size and shape of adult (3–5 months) *CD24* mutant and wild-type endplates.

**AM1-43 Optical Imaging to Visualize Vesicle Cycling.** Endplates were labeled by incubation with the AChR antibody (mAb 35; Developmental Studies Hybridoma Bank, Iowa City, IA) conjugated with Alexa 546 (Molecular Probes) for 1 hr, and AM1–43 dye uptake experiments were performed as described in ref. 18.

We thank Silvia Arber and Tom Jessell (both of Columbia University, New York) for providing us with *HB9$^{cre}$*, *Isl1$^{cre}$*, and *Isl2$^{loxP}$*-stop-loxP-DTA mice; Peter Nielsen (Max Planck Institute, Freiburg, Germany) and Yang Liu (Ohio State University, Columbus) for providing us with *CD24* mutant mice; and Carmen Birchmeier (Max Delbrück Institute, Berlin) for providing us with *nrg-1* mutant mice. The microarray work was completed through the National Institute of Neurological Disorders and Stroke and National Institute of Mental Health Microarray Consortium (http://arrayconsortium.tgen.org) with the assistance of Zugen Chen. This work was supported by National Institutes of Health Grants NS41311 and NS27963 (to S.J.B.) and NS23678 (to L.T.L.). M.J. was supported by the Slovenian Research Agency.

1. Merlie, J. P. & Sanes, J. R. (1985) *Nature* **317,** 66–68.
2. Jasmin, B. J., Lee, R. K. & Rotundo, R. L. (1993) *Neuron* **11,** 467–477.
3. Valenzuela, D. M., Stitt, T. N., DiStefano, P. S., Rojas, E., Mattsson, K., Compton, D. L., Nunez, L., Park, J. S., Stark, J. L., Gies, D. R., *et al.* (1995) *Neuron* **15,** 573–584.
4. Gramolini, A. O., Dennis, C. L., Tinsley, J. M., Robertson, G. S., Cartaud, J., Davies, K. E. & Jasmin, B. J. (1997) *J. Biol. Chem.* **272,** 8117–8120.
5. Schaeffer, L., de Kerchove d'Exaerde, A. & Changeux, J. P. (2001) *Neuron* **31,** 15–22.
6. DeChiara, T. M., Bowen, D. C., Valenzuela, D. M., Simmons, M. V., Poueymirou, W. T., Thomas, S., Kinetz, E., Compton, D. L., Rojas, E., Park, J. S., *et al.* (1996) *Cell* **85,** 501–512.
7. Gautam, M., Noakes, P. G., Moscoso, L., Rupp, F., Scheller, R. H., Merlie, J. P. & Sanes, J. R. (1996) *Cell* **85,** 525–535.
8. Moscoso, L. M., Merlie, J. P. & Sanes, J. R. (1995) *Mol. Cell. Neurosci.* **6,** 80–89.
9. Hebb, C. O., Krnjevic, K. & Silver, A. (1964) *J. Physiol. (London)* **171,** 504–513.
10. Kay, R., Rosten, P. M. & Humphries, R. K. (1991) *J. Immunol.* **147,** 1412–1416.
11. Wenger, R. H., Ayane, M., Bose, R., Kohler, G. & Nielsen, P. J. (1991) *Eur. J. Immunol.* **21,** 1039–1046.
12. Rimer, M., Prieto, A. L., Weber, J. L., Colasante, C., Ponomareva, O., Fromm, L., Schwab, M. H., Lai, C. & Burden, S. J. (2004) *Mol. Cell. Neurosci.* **26,** 271–281.
13. Yang, X., Arber, S., William, C., Li, L., Tanabe, Y., Jessell, T. M., Birchmeier, C. & Burden, S. J. (2001) *Neuron* **30,** 399–410.
14. Yang, X., Li, W., Prescott, E. D., Burden, S. J. & Wang, J. C. (2000) *Science* **287,** 131–134.
15. Lin, W., Burgess, R. W., Dominguez, B., Pfaff, S. L., Sanes, J. R. & Lee, K. F. (2001) *Nature* **410,** 1057–1064.
16. Nielsen, P. J., Lorenz, B., Muller, A. M., Wenger, R. H., Brombacher, F., Simon, M., von der Weid, T., Langhorne, W. J., Mossmann, H. & Kohler, G. (1997) *Blood* **89,** 1058–1067.
17. Polo-Parada, L., Bose, C. M., Plattner, F. & Landmesser, L. T. (2004) *J. Neurosci.* **24,** 1852–1864.
18. Polo-Parada, L., Bose, C. M. & Landmesser, L. T. (2001) *Neuron* **32,** 815–828.
19. Polo-Parada, L., Plattner, F., Bose, C. & Landmesser, L. T. (2005) *Neuron* **46,** 917–931.
20. Brigant, J. L. & Mallart, A. (1982) *J. Physiol. (London)* **333,** 619–636.
21. Chan, S. A., Polo-Parada, L., Landmesser, L. T. & Smith, C. (2005) *J. Neurophysiol.* **94,** 1037–1047.
22. Kishi, M., Kummer, T. T., Eglen, S. J. & Sanes, J. R. (2005) *J. Cell Biol.* **169,** 355–366.
23. Sammar, M., Aigner, S. & Altevogt, P. (1997) *Biochim. Biophys. Acta* **1337,** 287–294.
24. Verstreken, P., Ly, C. V., Venken, K. J., Koh, T. W., Zhou, Y. & Bellen, H. J. (2005) *Neuron* **47,** 365–378.
25. Belvindrah, R., Rougon, G. & Chazal, G. (2002) *J. Neurosci.* **22,** 3594–3607.
26. Figarella-Branger, D., Moreau, H., Pellissier, J. F., Bianco, N. & Rougon, G. (1993) *Acta Neuropathol.* **86,** 275–284.
27. Nieoullon, V., Belvindrah, R., Rougon, G. & Chazal, G. (2005) *Mol. Cell. Neurosci.* **28,** 462–474.
28. Aigner, S., Ramos, C. L., Hafezi-Moghadam, A., Lawrence, M. B., Friederichs, J., Altevogt, P. & Ley, K. (1998) *FASEB J.* **12,** 1241–1251.
29. Stefanova, I., Horejsi, V., Ansotegui, I. J., Knapp, W. & Stockinger, H. (1991) *Science* **254,** 1016–1019.
30. Sammar, M., Gulbins, E., Hilbert, K., Lang, F. & Altevogt, P. (1997) *Biochem. Biophys. Res. Commun.* **234,** 330–334.
31. Kadmon, G., von Bohlen und Halbach, F., Horstkorte, R., Eckert, M., Altevogt, P. & Schachner, M. (1995) *Eur. J. Neurosci.* **7,** 993–1004.
32. Foster-Barber, A. & Bishop, J. M. (1998) *Proc. Natl. Acad. Sci. USA* **95,** 4673–4677.
33. Linstedt, A. D., Vetter, M. L., Bishop, J. M. & Kelly, R. B. (1992) *J. Cell Biol.* **117,** 1077–1084.
34. Janz, R. & Südhof, T. C. (1998) *J. Biol. Chem.* **273,** 2851–2857.
35. Cheng, L. & Wong, W. H. (2003) in *The Analysis of Gene Expression Data: Methods and Software*, eds. Parmigiani, G., Garett, E. S., Irizarry, R. & Zeger, S. L. (Springer, New York), pp. 12–141.
36. Herbst, R., Avetisova, E. & Burden, S. J. (2002) *Development (Cambridge, U.K.)* **129,** 5449–5460.
37. Alterman, L. A., Crispe, I. N. & Kinnon, C. (1990) *Eur. J. Immunol.* **20,** 1597–1602.